Nano Research
2023, 16(2): 2271–2277

ISSN 1998-0124 CN 11-5974/O4
https://doi.org/10.1007/s12274-022-5055-2

Research Article

# Counterbalancing of electron and hole transfer in quantum dots for enhanced photocatalytic $H_2$ evolution

Ping Wang[1,2,3,§] (✉), Wenwu Shi[2,4,§], Na Jin[2], Zhenyang Liu[2], Yongchen Wang[5], Tong Cai[2], Katie Hills-Kimball[2], Hanjun Yang[2], Xiaotian Yang[1,6] (✉), Yongdong Jin[3], Xinzhong Wang[4] (✉), Jing Zhao[4], and Ou Chen[2] (✉)

[1] *Key Laboratory of Preparation and Applications of Environmental Friendly Material of the Ministry of Education, College of Chemistry, Jilin Normal University, Changchun 130103, China*
[2] *Department of Chemistry, Brown University, Providence, Rhode Island 02912, USA*
[3] *State Key Laboratory of Electroanalytical Chemistry, Changchun Institute of Applied Chemistry, Chinese Academy of Sciences, Changchun 130022, China*
[4] *Institute of Information Technology, Shenzhen Institute of Information Technology, Shenzhen 518172, China*
[5] *Department of Chemistry, University of Connecticut, Storrs, Connecticut 06269-3060, USA*
[6] *Key Laboratory for Comprehensive Energy Saving of Cold Regions Architecture of the Ministry of Education, Jilin Jianzhu University, Changchun 130118, China*
[§] *Ping Wang and Wenwu Shi contributed equally to this work.*



**Received:** 27 July 2022 / **Revised:** 12 September 2022 / **Accepted:** 14 September 2022

## ABSTRACT

In-depth understandings of charge carrier transfer dynamics in any artificial catalytic system are of critical importance for the future design of highly efficient photocatalysts. Herein, we synthesized sub-monolayer ZnSe partial-shell coated CdSe/CdS core/shell quantum dots in a controlled fashion. The ZnSe decorated quantum dots were employed as a model catalyst for photogeneration of $H_2$ under light illumination. Both theoretical calculations and experimental results unravel that the growth of ZnSe partial-shell would retard the photogenerated electron transfer, and meanwhile, accelerate the corresponding hole migration process during the $H_2$ photogeneration reaction in the artificial photocatalytic system. As such, the performance of the relevant photocatalytic system can be modulated and optimized, and accordingly, a plausible underlying mechanism is rationalized.

## KEYWORDS

photocatalysis, hydrogen, CdSe/CdS, quantum dots, ZnSe, partial coating

## 1 Introduction

Efficient production of hydrogen ($H_2$) from water and sunlight as a clean energy source has been considered as a promising approach to mitigate the global environmental crisis and energy shortage, and therefore, has gained extensive attention over decades [1–13]. To realize efficient photogeneration of $H_2$, various multicomponent artificial systems comprised of light absorbers, cocatalysts, and hole scavengers have been proposed and developed [14–16]. Significant amount of efforts have been particularly devoted to the investigation of light absorbers, which play a vital role in absorbing and converting incident photons into electrons and holes for the subsequent $H_2$ generation reaction [17–23]. Among various choices of light absorbers, colloidal semiconductor quantum dots (QDs) have been recognized as one of the most promising candidates owing to their merits of high photostability, efficient and broad light absorption, and tunable composition with controlled band structures for photocarrier dynamics optimizations [24–26].

Deliberate tailoring of geometrical parameters, surface states, and compositions of QDs has been identified as an effective means to manipulate the electron/hole transfer behavior and redox potentials of the photogenerated charge carriers, thus enhancing the performance in $H_2$ photogeneration reactions [27–30]. For example, through fine-tuning of the CdSe core size as well as the length of CdSe/CdS dot-in-rod heterostructural nanorod, the photocatalytic activity of $H_2$ evolution can be significantly improved under optimal conditions [31]. Further selective etching of this structure to directly expose CdSe core to the reaction environment could result in over three-fold activity enhancement, which was attributed to the unobstructed hole transfer to the particle surfaces [32]. Another interesting example is the ZnSe/CdS/Pt and ZnTe/CdS/Pt heterostructural QDs with similar sizes, morphology, and band alignment (i.e., type-II). Their $H_2$ photogeneration activities exhibit, however, a striking difference (ZnSe/CdS/Pt >> ZnTe/CdS/Pt) [33]. This activity difference is ascribed to the different valence hole energies of ZnSe and ZnTe domains relative to the highest occupied molecular orbital (HOMO) level of the surface ligand, which results in a distinct hole transfer behavior to the sacrificial electron donor. Despite

Address correspondence to Ping Wang, ping@jlnu.edu.cn; Xiaotian Yang, hanyxt@163.com; Xinzhong Wang, wangxz@sziit.edu.cn; Ou Chen, ouchen@brown.edu

these exciting results, insightful understandings of the charge carrier dynamics by elaborate designs of QD photocatalysts are still highly desired due to the potential guidance it may provide to further boost the reaction efficiency of these QD-based photocatalytic artificial systems.

In this work, CdSe/CdS core/shell QDs were employed as a host, where the photoinduced hole and electron are known mainly in the core and shell region, respectively [34]. Sub-monolayer (ML) of ZnSe partial-shell, with an appropriate band alignment [35, 36], was then grown onto the host QDs in a controlled manner to investigate the influence of ZnSe partial-shell decoration on the relevant charge transfer dynamics. Results from density functional theory (DFT) calculations, photoluminescence (PL) lifetime, and PL quenching measurements have shown that the CdSe/CdS QDs with ZnSe partial-shell coating exhibit an opposite effect on the transfer characteristics of electron and hole. As such, the performance of the relevant artificial $H_2$ photogeneration system was modulated by this charge transfer behavior variation. Furthermore, the corresponding underlying mechanism is rationally proposed.

## 2 Results and discussion

Sub-ML ZnSe partial-shell decorated CdSe/CdS core/shell QDs were synthesized by a two-step protocol. The synthetic details can be found in the Electronic Supplementary Material (ESM). Briefly, CdSe/CdS core/shell QDs with a 2.9 nm CdSe core (the first exciton peak at 540 nm) and 4 MLs of CdS shell were first synthesized according to a previously published method [37, 38]. Then, the obtained core/shell QDs were further coated with a sub-ML ZnSe partial-shell (see the ESM for details). The ZnSe partial-shell decorated QD samples are denoted as CdSe/CdS/$ZnSe_L$ and CdSe/CdS/$ZnSe_H$, where the subscripts, i.e., L and H, stand for the low (0.2 ML) and high (1.0 ML) ZnSe precursor feeding amount, respectively. Ultraviolet–visible (UV–Vis) and PL spectra show that after CdS shell growth, the first excitonic absorption peak of the QDs red-shifted from 540 to 577 nm, and the PL peak red-shifted from 555 to 591 nm (Fig. 1(a)), consistent with the quasi-type-II band structural alignment of the CdSe/CdS core/shell structure [38–40]. During the CdS shell growth process, the PL quantum yield (PL QY) increased from ~ 3% to over 80%, indicating high-quality shell formation [38]. Further coating of ZnSe partial-shell did not induce any obvious changes of either the absorption or emission properties (Fig. 1(a)), revealing a minimal effect on the optical characteristics of the host QDs. In contrast to the conventional CdSe/CdS/ZnSe core/shell/shell QDs, which typically exhibit a dual emission profile induced by its unique type-I/type-II hetero-bandgap-alignment [35, 41], the intact optical properties observed in our case validate a sub-ML partial-shell coating of ZnSe. The sub-ML shell coating was further confirmed by the X-ray diffraction (XRD) measurements, where the wurtzite crystal structure of the final CdSe/CdS/ZnSe QD samples was maintained with no measurable diffraction peak shifting (Fig. 1(b)). X-ray photoelectron spectroscopy (XPS) spectra show two peaks centered at 1,021.6 and 1,044.5 eV, which can be assigned to Zn $2p_{1/2}$ and Zn $2p_{3/2}$ orbitals of divalent $Zn^{2+}$ cations [42, 43]. The enhanced peak intensities for the CdSe/CdS/$ZnSe_H$ QDs agree well with the increased surface Zn content as compared to the CdSe/CdS/$ZnSe_L$ QD sample (Fig. 1(c)). Inductively coupled plasma-atomic emission spectroscopy (ICP-AES) technique was further employed to accurately determine the amount of ZnSe partial-shell on the CdSe/CdS QD hosts. The results reveal that the atomic ratio of Zn ($Zn_{atom-r}$, calculated by [Zn]/([Zn] + [Se] + [S] + [Cd])) is 3.49% and 9.14% for the CdSe/CdS/$ZnSe_L$ and CdSe/CdS/$ZnSe_H$ QD samples, respectively (Fig. 1(d) and Table S1 in the ESM), which equal to 0.18 and 0.52 ML ZnSe shell (see calculation details in the ESM).

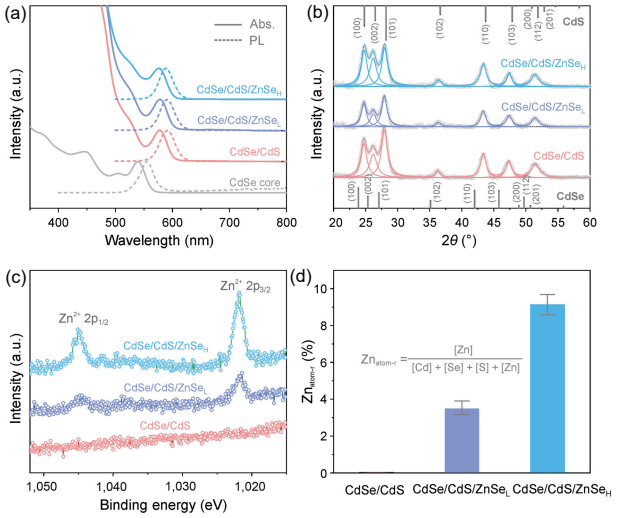


**Figure 1** (a) UV–Vis and PL spectra of CdSe core, CdSe/CdS, CdSe/CdS/$ZnSe_L$, and CdSe/CdS/$ZnSe_H$ core/shell QDs; (b) XRD patterns of CdSe/CdS, CdSe/CdS/$ZnSe_L$, and CdSe/CdS/$ZnSe_H$ core/shell QDs. The sticks indicate the positions of standard XRD peaks of bulk wurtzite CdSe (bottom) and CdS (top); and (c) XPS spectra of Zn 2p and (d) Zn atomic ratio ($Zn_{atom-r}$) (calculation based on the ICP-AES results) of CdSe/CdS, CdSe/CdS/$ZnSe_L$, and CdSe/CdS/$ZnSe_H$ core/shell QDs.

Transmission electron microscopy (TEM) measurements show that nearly monodispersed spherical QDs with a mean size of 5.6 ± 0.7 nm were obtained after CdS shell growth (Figs. S1(a) and S1(b) in the ESM), which corresponds to a CdS shell thickness of ~ 4 MLs [40, 44]. After coating with ZnSe, both CdSe/CdS/$ZnSe_L$ and CdSe/CdS/$ZnSe_H$ samples show nearly no change to the size and morphology of the CdSe/CdS host QDs, or any visible ZnSe crystalline domains on the particle surfaces (Figs. 2(a) and 2(b), and Figs. S1(c)–S1(f) in the ESM). This result is consistent with the sub-ML ZnSe partial-shell coatings for both samples (the thickness of a full ML of ZnSe shell equals 0.33 nm) [45]. High-resolution TEM (HRTEM) image of a representative QD shows good crystallinity with a measured lattice spacing of 3.6 Å (inset of Fig. 2(b)), which is consistent with the *d*-spacing between two adjacent (100) crystal planes of hexagonal CdS, in line with the wurtzite crystal phase of the QDs (Fig. 1(b)) [46]. High-angle annular dark-field scanning TEM (HAADF-STEM) characterization was applied to reveal the atomic distributions of the ZnSe partial-shell decorated CdSe/CdS QDs (Figs. 2(c) and 2(d)). Elemental mapping results show that Cd, Se, S, and Zn are homogeneously distributed throughout the entire QD (Fig. 2(d) and Figs. S2 and S3 in the ESM), demonstrating the uniform coating of ZnSe partial-shell layer. All the above results signify the successful growth of sub-ML ZnSe partial-shell on the CdSe/CdS core/shell host QDs without influencing the morphology, optical characteristic, and crystal structure of the host particles.

DFT calculations were performed to unveil the electronic structure variations and the effect of ZnSe partial-shell coating on the charge carrier transfer behavior of the relevant QDs. Four different heterostructure configurations with ZnSe surface coating ratios (i.e., the ZnSe coverage percentage on the surface CdS) of 0.0, 0.25, 0.50, and 1.0 were constructed for the calculation (Figs. S4(a)–S4(d) in the ESM, see the ESM for calculation details). The calculation results show that there is only a slight variation (< 10 meV) of the bandgap energy ($E_g$) for the structural configurations with partial ZnSe coatings (i.e., coating ratios of 0.25 and 0.50) compared to that of the configuration without ZnSe coating (Figs. 3(a)–3(d) and Table 1). After reaching a full layer of

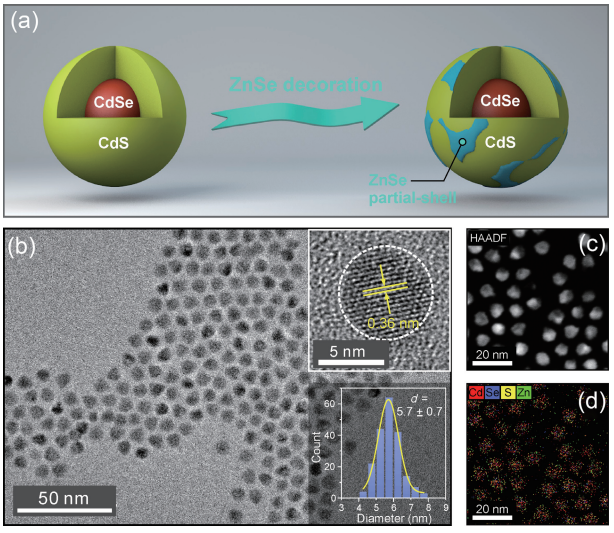


**Figure 2** (a) Schematic illustration of the growth of ZnSe partial-shell onto the host CdSe/CdS core/shell QDs; (b) TEM and HRTEM images (inset), and size distribution histogram (inset) of CdSe/CdS/$ZnSe_L$ core/shell QDs; and (c) HAADF-STEM image of CdSe/CdS/$ZnSe_L$ core/shell QDs and (d) corresponding overlapping elemental mapping of Cd, Se, S, and Zn, respectively.

ZnSe coating (i.e., coating ratios of 1.0), a larger decrease of $E_g$ (i.e., 21 meV) was obtained (Fig. 3(d) and Table 1). These calculation results manifest a minimal electronic band structure perturbation by the ZnSe partial-shell coating, consistent with our experimental observations (Fig. 1(a)). It should be noted that the calculated $E_g$ values (~ 0.81–0.83 eV) are much smaller than that obtained through the Tauc plot analyses based on the UV–Vis absorption spectra (2.08 eV, Fig. 1(a) and Fig. S5 in the ESM). Such bandgap underestimation has been commonly observed in similar kinds of standard DFT calculations mainly caused by the employed generalized gradient approximation method [47, 48]. Nevertheless, the variation trend of the calculated $E_g$ values should be still valid.

Next, we investigated charge density difference and charge distribution characteristics, which are considered to also have a key influence on the activity of the photocatalyst with different structural configurations [49]. The calculation results indicate the variation of ZnSe coating does not obviously alter the charge distribution (Figs. 3(e)–3(h)) or charge depletion and accumulation (Figs. S4(e)–S4(h) in the ESM) characteristics of the relevant structures. This was further supported by the similar projected density of states (DOS) (Figs. 3(a)–3(d)). For all cases, the conduction band minimum (CBM) is dominantly composed of the Cd 5s and S 3p orbitals, while the valence band maximum (VBM) mainly originates from Se 4p, S 3p, and Cd 5d orbitals, and with small contributions from Zn 3p and 3d orbitals.

It is known that photo-induced charge transfer dynamics of QDs are crucial and directly related to their photocatalytic performances in various photoreactions [23, 50, 51]. Therefore, we calculated the electron ($\mu_e$) and hole ($\mu_h$) mobilities for the four different structural configurations to uncover the ZnSe partial-shell coating effect. The results show that, for the CdSe/CdS core/shell structure, the electron mobility, i.e., $\mu_e$, along $x$ ($y$) direction is 19,925.18 (3,800.02) $cm^2 \cdot V^{-1} \cdot s^{-1}$ (as indicated in Table 1), while for that of hole mobility, i.e., $\mu_h$ is only 269.02 (147.42) $cm^2 \cdot V^{-1} \cdot s^{-1}$ (Table 1). The distinct difference between $\mu_e$ and $\mu_h$ is due to the much smaller effective mass ($m^*$) of the electron than that of the hole (Table S2 in the ESM), as also reported by previous theoretical and experimental studies [35, 52, 53]. With increasing the ZnSe surface coating ratio, $\mu_e$ along both $x$ and $y$ directions gradually decreased, while a clear opposite trend for hole mobility ($\mu_h$ increased) was observed as listed in Table 1. Taking all together, our DFT calculations reveal that partial coating of ZnSe onto the host CdSe/CdS core/shell QDs only has a minor effect on the relevant electronic band structures, yet significantly alters the electron and hole transfer characteristics, which would subsequently influence the photocatalytic performance of the corresponding structures.

To gain more understandings of the charge carrier dynamics in our photocatalytic system, a time-resolved PL decay analysis was performed (see details in the ESM), which has proven to be an effective protocol to evaluate the charge transfer rate of the relevant photocatalytic systems [54–56]. As shown in Fig. S6 in the ESM, all the PL decay traces can be fitted into tri-exponential decay kinetics and the corresponding lifetime data are summarized in Tables S3 and S4 in the ESM. It has been reported that efficient Ni-based cocatalyst can be formed *in-situ* by introducing $Ni^{2+}$ ions into CdSe/CdS core/shell QDs-based catalytic system and ascorbic acid (AA) can be used as an effective hole scavenger [30]. Therefore, the same ingredients ($Ni^{2+}$ ion and AA) were employed in our study. The PL decay analysis results show that the average lifetimes for all the samples (i.e., CdSe/CdS, CdSe/CdS/$ZnSe_L$, and CdSe/CdS/$ZnSe_H$ QDs) exhibit a universal

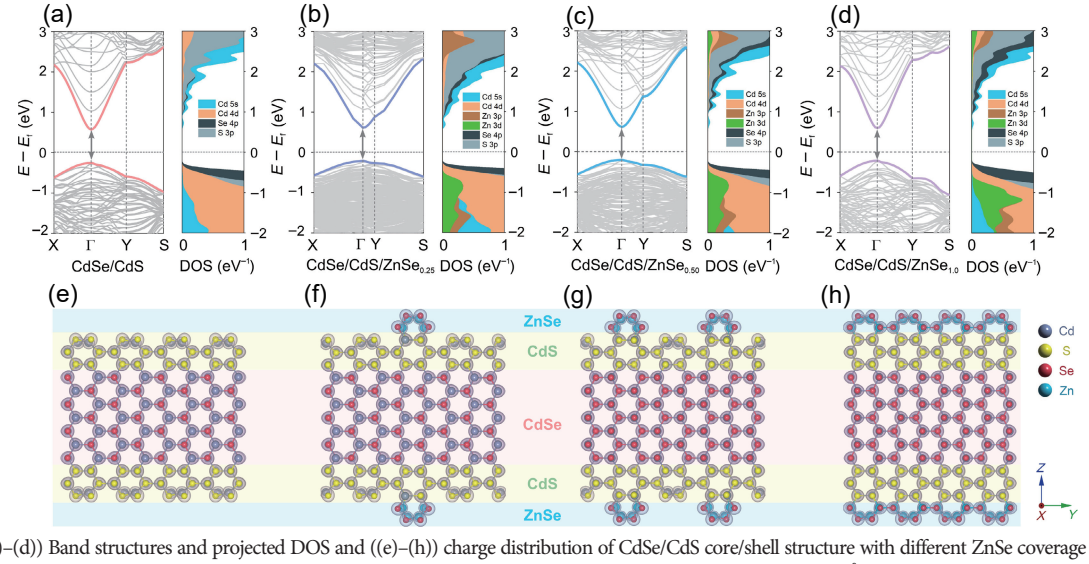


**Figure 3** ((a)–(d)) Band structures and projected DOS and ((e)–(h)) charge distribution of CdSe/CdS core/shell structure with different ZnSe coverage (coating ratios of 0.0, 0.25, 0.50, and 1.0), where the light pink isosurfaces ((e)–(h)) indicate the charge distribution with unit of 0.06 e·Å$^{-3}$. The Fermi energy ($E_f$) was set to zero as indicated by the gray dashed line in ((a)–(d)).

**Table 1** Calculated charge carrier mobility ($\mu$) of electron and hole along $x$ and $y$ directions, and bandgap ($E_g$) of CdSe/CdS core/shell structure with different ZnSe coating ratios

| ZnSe coating ratio | $\mu_e$ ($cm^2 \cdot V^{-1} \cdot s^{-1}$) (along $x$ direction) | $\mu_e$ ($cm^2 \cdot V^{-1} \cdot s^{-1}$) (along $y$ direction) | $\mu_h$ ($cm^2 \cdot V^{-1} \cdot s^{-1}$) (along $x$ direction) | $\mu_h$ ($cm^2 \cdot V^{-1} \cdot s^{-1}$) (along $y$ direction) | $E_g$ (eV) |
|---|---|---|---|---|---|
| 0.0 | 19,925.18 | 3,800.02 | 269.02 | 147.42 | 0.831 |
| 0.25 | 17,724.33 | 3,167.11 | 280.95 | 309.51 | 0.827 |
| 0.5 | 13,570.36 | 2,827.37 | 356.96 | 462.47 | 0.823 |
| 1.0 | 10,854.11 | 2,472.92 | 408.74 | 693.09 | 0.810 |

decrease after adding either $Ni^{2+}$ ions (25 μM) or AA (0.1 M) into the solution (Fig. S6 and Tables S3 and S4 in the ESM). This PL lifetime shortening effect is attributed to the photoinduced electron (hole) injection from the QDs into the Ni-based cocatalyst (AA) [54]. The corresponding photocarrier (electron or hole) transfer rate constant ($k$) can be quantitatively determined by the following equation [54]

$$k = 1/\tau_1 - 1/\tau_0$$

where $\tau_0$ and $\tau_1$ refer to the average lifetime of the QDs before and after introducing the quenchers ($Ni^{2+}$ ion and AA), respectively.

The calculation results show that with the introduction of the ZnSe partial-shell, the electron transfer rate constant ($k_{ET}$) gradually decreased from $2.2 \times 10^7$ to $0.56 \times 10^7$ $s^{-1}$; while the corresponding hole transfer rate constant ($k_{HT}$) was doubled from $2.1 \times 10^7$ to $4.3 \times 10^7$ $s^{-1}$ (Fig. 4(a)). This decrease (increase) in the electron (hole) transfer rate agrees well with the DFT calculations for the charge carrier mobilities as listed in Table 1. In addition, by varying the concentration of the added quenchers ($Ni^{2+}$ ion and AA), the concentration-dependent PL intensity decrease can be fitted into the Stern–Volmer model (see details in the ESM, Figs. S7 and S8 in the ESM) [57]. The changes of the calculated electron- and hole-related quenching rate constant exhibit the same trend as that obtained from the PL decay analyses (Fig. 4(a) and Table S5 in the ESM). Altogether, both the PL decay lifetime and PL intensity analyses results, along with the DFT calculations confirm that the sub-ML ZnSe partial-shell modification to the pristine CdSe/CdS core/shell QDs can decelerate (accelerate) electron (hole) transfer rate from the QDs to the Ni-based cocatalyst (AA).

The above investigations affirm that the ZnSe decoration would retard the electron transfer and meanwhile facilitate the hole

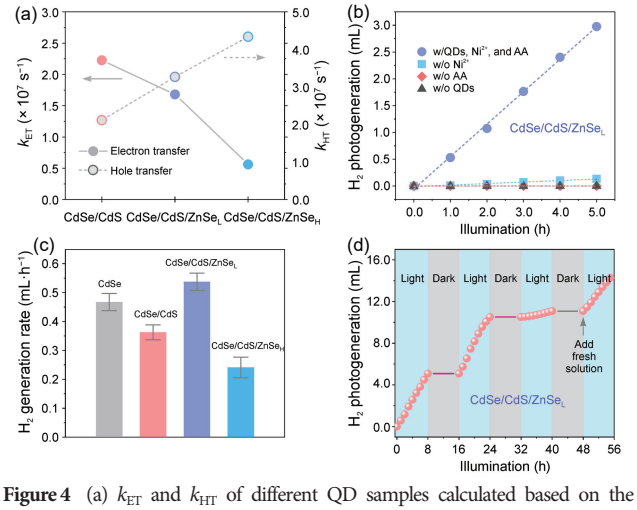


**Figure 4** (a) $k_{ET}$ and $k_{HT}$ of different QD samples calculated based on the corresponding emission lifetime variation before and after introducing quenchers (see the ESM); (b) $H_2$ photogeneration of the system versus illumination (405 nm) time under different conditions; (c) comparison of the rate of $H_2$ photogeneration for the different QD-based systems under the illumination of 405 nm light; and (d) long-term light on/off cycles of $H_2$ photogeneration using CdSe/CdS/ZnSe$_L$ core/shell QD as the photocatalyst.

migration of the host CdSe/CdS core/shell QDs. Subsequently, the influence of corresponding variations on the relevant photocatalytic activity was evaluated in photocatalytic $H_2$ evolution reactions. To perform the photocatalytic reaction, all the QDs studied here were first subjected to a ligand exchange process to make them water-soluble using inorganic $S^{2-}$ ions as the ligands (see details in the ESM), which has proven to be an effective ligand for photocatalytic $H_2$ evolution [30, 58]. The successful organic-to-inorganic ligand exchanges were confirmed by the Fourier transform infrared (FTIR) spectroscopy measurements evidenced by, e.g., the significantly weakened C–H stretching vibrational modes (asymmetric: 2,917 $cm^{-1}$ and symmetric: 2,848 $cm^{-1}$) of the native organic ligand molecules (i.e., oleate and oleylamine, Fig. S9 in the ESM). The $S^{2-}$ capped QDs were then applied as photocatalysts for $H_2$ evolution reaction. Figure 4(b) shows the $H_2$ evolutions over reaction time using the CdSe/CdS/ZnSe$_L$ QDs as the photocatalysts (with 405 nm incident light) under different reaction conditions. The results clearly show that a good photoactivity with an $H_2$ generation rate of 0.54 mL·$h^{-1}$ can be observed only when the reaction solution simultaneously contains the QDs photocatalyst, $Ni^{2+}$ co-catalyst, and AA hole scavenger (Fig. 4(b)). Whereas, no activities were obtained when the reaction solution was lack of either QDs or AA and a negligible activity (0.03 mL·$h^{-1}$) was observed when no $Ni^{2+}$ co-catalyst was in the solution (Fig. 4(b)). These results unambiguously demonstrate the requirement and essential roles of QDs, $Ni^{2+}$, and AA for an efficient $H_2$ photogeneration reaction.

Next, we compared the photocatalytic performance of different QD samples. As shown in Fig. 4(c), the $H_2$ evolution rate of the host CdSe/CdS QDs (0.36 mL·$h^{-1}$) is lower than that of CdSe core-only QDs (0.47 mL·$h^{-1}$). The lower activity of the CdSe/CdS QDs can be ascribed to the unbalanced confinements to the photogenerated electron (weak confinement) and hole (strong confinement) due to the quasi-type-II band alignment, in good accordance with the previous reports [57]. The activity of CdSe/CdS/ZnSe$_H$ QDs was 0.24 mL·$h^{-1}$, significantly lower than that of the CdSe/CdS/ZnSe$_L$ sample which showed the best catalytic performance with an $H_2$ photogeneration rate of 0.54 mL·$h^{-1}$ (Figs. 4(b) and 4(c)). The measured apparent quantum yield (AQY) of 9.1% (405 nm incident light, 27.4 mW·$cm^{-2}$) for the CdSe/CdS/ZnSe$_L$ QD relevant photocatalytic system is 50.0% and 14.9% higher than that of the host CdSe/CdS QDs and CdSe core-only QDs, respectively. To confirm the photon-induced reactivity and examine the stability of the QD photocatalysts, a long-term measurement with consecutive light on/off cycles was carried out. As shown in Fig. 4(d), the $H_2$ photogeneration rate maintained nearly identical (~ 0.58 mL·$h^{-1}$) during the first two cycles, and showed an obvious decrease during the third cycle (0.1 mL·$h^{-1}$). The decrease was likely attributed to the possible surface deactivation of QDs as previously reported [58], evidenced by the recovery of the $H_2$ generation rate to 0.48 mL·$h^{-1}$ (the slight decrease was caused by a minor loss of QDs during the recycling process) after purification and recollection of the QDs for a new set of photoreactions (with freshly prepared $Ni^{2+}$ and AA) (Fig. 4(d)). This result demonstrates the superior stability and

recyclability of the obtained CdSe/CdS/ZnSe QDs for photocatalytic reaction.

For the QD-catalyzed $H_2$ photogeneration artificial systems studied here, under identical reaction conditions, it is reasonable to hypothesize that the variation of catalytic efficiency for different QD catalysts is attributed to the different charge carrier dynamics induced by altered bandgap alignments. Specifically, for the CdSe/CdS core/shell QDs, once excited, the hole is largely confined in the core region and difficult to tunnel through the CdS shell and be consumed by hole scavenger, e.g., AA; whereas the corresponding electron can readily delocalize into the shell region and be captured by the $Ni^{2+}$-based co-catalyst for $H_2$ production (Fig. 5, left). These unbalanced electron and hole photo-dynamics limit the photocatalytic performance of CdSe/CdS core/shell QDs in $H_2$ generation reaction. Such an unbalance can be mitigated by the sub-ML ZnSe partial-shell coating, which provides a slightly higher energy CBM and an in-between energy VBM as compared to the corresponding band edge energies (VBMs) of CdSe core and CdS shell (Fig. 5, right) [35]. This bandgap alignment difference leads to opposite effects on the transfer dynamics of photogenerated electron and hole: decreasing the electron transfer rate (reduced $k_{ET}$) due to the enlarged CB confinement; increasing the hole transfer rate (to the QD surface, enlarged $k_{HT}$) by softening the VB offset between CdSe and CdS (Fig. 5, right), thus improving the performance in photocatalytic $H_2$ generation reaction. Further increasing the ZnSe shell coating amount, the hindrance of electron transfer at the CB (increased CB confinement by the ZnSe shell) becomes the dominating factor, leading to the catalytic performance drop for $H_2$ evolution reaction. Both our experimental data and calculation results consistently validate our hypothesis.

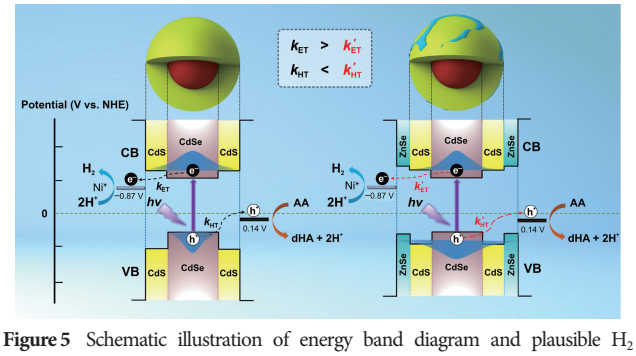


**Figure 5** Schematic illustration of energy band diagram and plausible $H_2$ photogeneration-related charge carrier transfer processes of CdSe/CdS QD-based catalytic system before (left) and after (right) ZnSe partial-shell coating (dHA refers to dehydroascorbic acid). The potential values of cocatalyst and electron donor were employed according to previous works [4, 30].

## 3 Conclusions

In conclusion, we studied the CdSe/CdS core/shell QDs decorated with sub-ML ZnSe partial-shell coating as photocatalysts for $H_2$ generation reaction under light excitation. We show that by coating 0.18 ML of ZnSe shell to CdSe/CdS QDs, an 50.0% enhancement compared to host CdSe/CdS QDs in catalytic efficiency for $H_2$ photogeneration reaction can be obtained. Further increasing the ZnSe partial-shell coating leads to an expected performance drop. Both experimental results and DFT calculation analyses convincingly manifest that the ZnSe partial-shell decoration on the CdSe/CdS core/shell QDs can balance the electron and hole photodynamics by slowing down the electron transfer and accelerating the hole migration, which is responsible for their photocatalytic performances. Our study represents the first demonstration to show that incomplete shell coating of QDs with desired hetero-bandgap alignment can be used as an effective means to modulate the performance of QD-based catalysts in photoreactions. The findings provide an insightful understanding of the QD charge carrier dynamics mediated catalytic process, offering valuable guidance for the future rational design of high-performance QD-based photocatalytic artificial systems.

## Acknowledgements

P. W. acknowledges the financial support from the China Scholarship Council (CSC) and the startup funding of Jilin Normal University (No. 2021036). X. T. Y. acknowledges the funding of Changbai Mountain industrial project R&D leading team, Jilin Provincial Department of Science and Technology, China. O. C. acknowledges the support from the Electron Microscopy Facility and NanoTools Facility at Brown University.

**Electronic Supplementary Material:** Supplementary material (experimental details, TEM results, and corresponding size distribution histogram of the relevant samples, HAADF-STEM results, specific atomic configuration, and charge distribution results; Tauc plot of the host CdSe/CdS core/shell QDs, PL lifetime decay results before and after introducing quenchers, PL quenching results with different concentration of quenchers, Stern–Volmer plots, FTIR spectra of different samples, table of ICP-AES data, table of DFT calculation-related data, PL lifetime data before and after introducing quenchers, Stern–Volmer slopes, PL lifetime, and calculated quenching rate constants of different QDs) is available in the online version of this article at https://doi.org/10.1007/s12274-022-5055-2.

## References

[1] Ran, J. R.; Zhang, J.; Yu, J. G.; Jaroniec, M.; Qiao, S. Z. Earth-abundant cocatalysts for semiconductor-based photocatalytic water splitting. *Chem. Soc. Rev.* **2014**, *43*, 7787–7812.

[2] Kudo, A.; Miseki, Y. Heterogeneous photocatalyst materials for water splitting. *Chem. Soc. Rev.* **2009**, *38*, 253–278.

[3] Fan, X. B.; Yu, S.; Hou, B.; Kim, J. M. Quantum dots based photocatalytic hydrogen evolution. *Isr. J. Chem.* **2019**, *59*, 762–773.

[4] Han, Z. J.; Qiu, F.; Eisenberg, R.; Holland, P. L.; Krauss, T. D. Robust photogeneration of $H_2$ in water using semiconductor nanocrystals and a nickel catalyst. *Science* **2012**, *338*, 1321–1324.

[5] Kandi, D.; Martha, S.; Parida, K. M. Quantum dots as enhancer in photocatalytic hydrogen evolution: A review. *Int. J. Hydrogen Energy* **2017**, *42*, 9467–9481.

[6] Wang, Y.; Ma, Y.; Li, X. B.; Gao, L.; Gao, X. Y.; Wei, X. Z.; Zhang, L. P.; Tung, C. H.; Qiao, L. J.; Wu, L. Z. Unveiling catalytic sites in a typical hydrogen photogeneration system consisting of semiconductor quantum dots and 3d-metal ions. *J. Am. Chem. Soc.* **2020**, *142*, 4680–4689.

[7] Wang, Q.; Domen, K. Particulate photocatalysts for light-driven water splitting: Mechanisms, challenges, and design strategies. *Chem. Rev.* **2020**, *120*, 919–985.

[8] Wolff, C. M.; Frischmann, P. D.; Schulze, M.; Bohn, B. J.; Wein, R.; Livadas, P.; Carlson, M. T.; Jäckel, F.; Feldmann, J.; Würthner, F. et al. All-in-one visible-light-driven water splitting by combining nanoparticulate and molecular co-catalysts on CdS nanorods. *Nat. Energy* **2018**, *3*, 862–869.

[9] Ben-Shahar, Y.; Scotognella, F.; Kriegel, I.; Moretti, L.; Cerullo, G.; Rabani, E.; Banin, U. Optimal metal domain size for photocatalysis with hybrid semiconductor-metal nanorods. *Nat. Commun.* **2016**, *7*, 10413.

[10] Liu, M.; Qiao, L. Z.; Dong, B. B.; Guo, S.; Yao, S.; Li, C.; Zhang, Z. M.; Lu, T. B. Photocatalytic coproduction of $H_2$ and industrial chemical over MOF-derived direct Z-scheme heterostructure. *Appl. Catal. B: Environ.* **2020**, *273*, 119066.

[11] Zhong, L. X.; Mao, B. D.; Liu, M.; Liu, M. Y.; Sun, Y. Q.; Song, Y. T.; Zhang, Z. M.; Lu, T. B. Construction of hierarchical photocatalysts by growing $ZnIn_2S_4$ nanosheets on Prussian blue analogue-derived bimetallic sulfides for solar co-production of $H_2$ and organic chemicals. *J. Energy Chem.* **2021**, *54*, 386–394.
[12] Guo, S.; Kong, L. H.; Wang, P.; Yao, S.; Lu, T. B.; Zhang, Z. M. Switching excited state distribution of metal-organic framework for dramatically boosting photocatalysis. *Angew. Chem., Int. Ed.* **2022**, *61*, e202206193.
[13] Lan, Q.; Jin, S. J.; Yang, B. H.; Zhao, Q.; Si, C. L.; Xie, H. Q.; Zhang, Z. M. Metal-oxo cluster catalysts for photocatalytic water splitting and carbon dioxide reduction. *Trans. Tianjin Univ.* **2022**, *28*, 214–225.
[14] Li, X. B.; Tung, C. H.; Wu, L. Z. Semiconducting quantum dots for artificial photosynthesis. *Nat. Rev. Chem.* **2018**, *2*, 160–173.
[15] Caputo, C. A.; Gross, M. A.; Lau, V. W.; Cavazza, C.; Lotsch, B. V.; Reisner, E. Photocatalytic hydrogen production using polymeric carbon nitride with a hydrogenase and a bioinspired synthetic Ni catalyst. *Angew. Chem., Int. Ed.* **2014**, *53*, 11538–11542.
[16] Wang, P.; Yang, Q. Q.; Xu, C.; Wang, B.; Wang, H.; Zhang, J. D.; Jin, Y. D. Magic-sized CdSe nanoclusters for efficient visible-light-driven hydrogen evolution. *Nano Res.* **2022**, *15*, 3106–3113.
[17] Li, Z. J.; Wang, J. J.; Li, X. B.; Fan, X. B.; Meng, Q. Y.; Feng, K.; Chen, B.; Tung, C. H.; Wu, L. Z. An exceptional artificial photocatalyst, $Ni_h$-CdSe/CdS core/shell hybrid, made *in situ* from CdSe quantum dots and nickel salts for efficient hydrogen evolution. *Adv. Mater.* **2013**, *25*, 6613–6618.
[18] Shemesh, Y.; Macdonald, J. E.; Menagen, G.; Banin, U. Synthesis and photocatalytic properties of a family of CdS-PdX hybrid nanoparticles. *Angew. Chem., Int. Ed.* **2011**, *50*, 1185–1189.
[19] Wang, F.; Liang, W. J.; Jian, J. X.; Li, C. B.; Chen, B.; Tung, C. H.; Wu, L. Z. Exceptional poly(acrylic acid)-based artificial [FeFe]-hydrogenases for photocatalytic $H_2$ production in water. *Angew. Chem., Int. Ed.* **2013**, *52*, 8134–8138.
[20] Wang, F.; Wang, W. G.; Wang, X. J.; Wang, H. Y.; Tung, C. H.; Wu, L. Z. A highly efficient photocatalytic system for hydrogen production by a robust hydrogenase mimic in an aqueous solution. *Angew. Chem., Int. Ed.* **2011**, *50*, 3193–3197.
[21] Li, Z. J.; Li, X. B.; Wang, J. J.; Yu, S.; Li, C. B.; Tung, C. H.; Wu, L. Z. A robust "artificial catalyst" *in situ* formed from CdTe QDs and inorganic cobalt salts for photocatalytic hydrogen evolution. *Energy Environ. Sci.* **2013**, *6*, 465–469.
[22] Brown, K. A.; Wilker, M. B.; Boehm, M.; Dukovic, G.; King, P. W. Characterization of photochemical processes for $H_2$ production by CdS nanorod-[FeFe] hydrogenase complexes. *J. Am. Chem. Soc.* **2012**, *134*, 5627–5636.
[23] Huang, J. E.; Mulfort, K. L.; Du, P. W.; Chen, L. X. Photodriven charge separation dynamics in CdSe/ZnS core/shell quantum dot/cobaloxime hybrid for efficient hydrogen production. *J. Am. Chem. Soc.* **2012**, *134*, 16472–16475.
[24] Vaneski, A.; Schneider, J.; Susha, A. S.; Rogach, A. L. Colloidal hybrid heterostructures based on II-VI semiconductor nanocrystals for photocatalytic hydrogen generation. *J. Photochem. Photobiol. C:Photochem. Rev.* **2014**, *19*, 52–61.
[25] Wilker, M. B.; Schnitzenbaumer, K. J.; Dukovic, G. Recent progress in photocatalysis mediated by colloidal II-VI nanocrystals. *Isr. J. Chem.* **2012**, *52*, 1002–1015.
[26] Yuan, Y. C.; Jin, N.; Saghy, P.; Dube, L.; Zhu, H.; Chen, O. Quantum dot photocatalysts for organic transformations. *J. Phys. Chem. Lett.* **2021**, *12*, 7180–7193.
[27] Li, Q. Y.; Zhao, F. J.; Qu, C.; Shang, Q. Y.; Xu, Z. H.; Yu, L.; McBride, J. R.; Lian, T. Q. Two-dimensional morphology enhances light-driven $H_2$ generation efficiency in CdS nanoplatelet-Pt heterostructures. *J. Am. Chem. Soc.* **2018**, *140*, 11726–11734.
[28] Han, G. Q.; Jin, Y. H.; Burgess, R. A.; Dickenson, N. E.; Cao, X. M.; Sun, Y. J. Visible-light-driven valorization of biomass intermediates integrated with $H_2$ production catalyzed by ultrathin Ni/CdS nanosheets. *J. Am. Chem. Soc.* **2017**, *139*, 15584–15587.
[29] Ben-Shahar, Y.; Scotognella, F.; Waiskopf, N.; Kriegel, I.; Dal Conte, S.; Cerullo, G.; Banin, U. Effect of surface coating on the photocatalytic function of hybrid CdS-Au nanorods. *Small* **2015**, *11*, 462–471.
[30] Wang, P.; Zhang, J.; He, H. L.; Xu, X. L.; Jin, Y. D. Efficient visible light-driven $H_2$ production in water by CdS/CdSe core/shell nanocrystals and an ordinary nickel-sulfur complex. *Nanoscale* **2014**, *6*, 13470–13475.
[31] Amirav, L.; Alivisatos, A. P. Photocatalytic hydrogen production with tunable nanorod heterostructures. *J. Phys. Chem. Lett.* **2010**, *1*, 1051–1054.
[32] Khon, E.; Lambright, K.; Khnayzer, R. S.; Moroz, P.; Perera, D.; Butaeva, E.; Lambright, S.; Castellano, F. N.; Zamkov, M. Improving the catalytic activity of semiconductor nanocrystals through selective domain etching. *Nano Lett.* **2013**, *13*, 2016–2023.
[33] Acharya, K. P.; Khnayzer, R. S.; O'Connor, T.; Diederich, G.; Kirsanova, M.; Klinkova, A.; Roth, D.; Kinder, E.; Imboden, M.; Zamkov, M. The role of hole localization in sacrificial hydrogen production by semiconductor-metal heterostructured nanocrystals. *Nano Lett.* **2011**, *11*, 2919–2926.
[34] Peng, X. G.; Schlamp, M. C.; Kadavanich, A. V.; Alivisatos, A. P. Epitaxial growth of highly luminescent CdSe/CdS core/shell nanocrystals with photostability and electronic accessibility. *J. Am. Chem. Soc.* **1997**, *119*, 7019–7029.
[35] Soni, U.; Pal, A.; Singh, S.; Mittal, M.; Yadav, S.; Elangovan, R.; Sapra, S. Simultaneous type-I/type-II emission from CdSe/CdS/ZnSe nano-heterostructures. *ACS Nano* **2014**, *8*, 113–123.
[36] Reiss, P.; Protière, M.; Li, L. Core/shell semiconductor nanocrystals. *Small* **2009**, *5*, 154–168.
[37] Tan, R.; Yuan, Y. C.; Nagaoka, Y.; Eggert, D.; Wang, X. D.; Thota, S.; Guo, P.; Yang, H. R.; Zhao, J.; Chen, O. Monodisperse hexagonal pyramidal and bipyramidal wurtzite CdSe-CdS core–shell nanocrystals. *Chem. Mater.* **2017**, *29*, 4097–4108.
[38] Chen, O.; Zhao, J.; Chauhan, V. P.; Cui, J.; Wong, C.; Harris, D. K.; Wei, H.; Han, H. S.; Fukumura, D.; Jain, R. K. et al. Compact high-quality CdSe-CdS core–shell nanocrystals with narrow emission linewidths and suppressed blinking. *Nat. Mater.* **2013**, *12*, 445–451.
[39] Wang, L.; Nonaka, K.; Okuhata, T.; Katayama, T.; Tamai, N. Quasi-type II carrier distribution in CdSe/CdS core/shell quantum dots with type I band alignment. *J. Phys. Chem. C* **2018**, *122*, 12038–12046.
[40] Li, J. J.; Wang, Y. A.; Guo, W. Z.; Keay, J. C.; Mishima, T. D.; Johnson, M. B.; Peng, X. G. Large-scale synthesis of nearly monodisperse CdSe/CdS core/shell nanocrystals using air-stable reagents via successive ion layer adsorption and reaction. *J. Am. Chem. Soc.* **2003**, *125*, 12567–12575.
[41] Ca, N. X.; Hien, N. T.; Tan, P. M.; Phan, T. L.; Thanh, L. D.; Do, P. V.; Bau, N. Q.; Lien, V. T. K.; Van, H. T. Tunable dual emission in type-I/type-II CdSe/CdS/ZnSe nanocrystals. *J. Alloys Compd.* **2019**, *791*, 144–151.
[42] Qiao, F.; Kang, R.; Liang, Q. C.; Cai, Y. Q.; Bian, J. M.; Hou, X. Y. Tunability in the optical and electronic properties of ZnSe microspheres via Ag and Mn doping. *ACS Omega* **2019**, *4*, 12271–12277.
[43] Yang, L.; Zhu, J. G.; Xiao, D. Q. Microemulsion-mediated hydrothermal synthesis of ZnSe and Fe-doped ZnSe quantum dots with different luminescence characteristics. *RSC Adv.* **2012**, *2*, 8179–8188.
[44] Yu, W. W.; Qu, L. H.; Guo, W. Z.; Peng, X. G. Experimental determination of the extinction coefficient of CdTe, CdSe, and CdS nanocrystals. *Chem. Mater.* **2003**, *15*, 2854–2860.
[45] Chen, D. A.; Zhao, F.; Qi, H.; Rutherford, M.; Peng, X. G. Bright and stable purple/blue emitting CdS/ZnS core/shell nanocrystals grown by thermal cycling using a single-source precursor. *Chem. Mater.* **2010**, *22*, 1437–1444.
[46] Ai, Z. Z.; Zhang, K.; Shi, D.; Chang, B.; Shao, Y. L.; Zhang, L.; Wu, Y. Z.; Hao, X. P. Band-matching transformation between CdS and BCNNTs with tunable p-n homojunction for enhanced photocatalytic pure water splitting. *Nano Energy* **2020**, *69*, 104408.
[47] Wróbel, J.; Kurzydłowski, K. J.; Hummer, K.; Kresse, G.; Piechota, J. Calculations of ZnO properties using the Heyd–Scuseria–Ernzerhof screened hybrid density functional. *Phys. Rev. B* **2009**, *80*, 155124.
[48] Luppi, M.; Ossicini, S. Ab initio study on oxidized silicon clusters

and silicon nanocrystals embedded in $SiO_2$:Beyond the quantum confinement effect. *Phys. Rev. B* **2005**, *71*, 035340.

[49] Liu, J. J. Origin of high photocatalytic efficiency in monolayer g-$C_3N_4$/CdS heterostructure: A hybrid DFT study. *J. Phys. Chem. C* **2015**, *119*, 28417–28423.

[50] Zhu, H. M.; Song, N. H.; Lv, H. J.; Hill, C. L.; Lian, T. Q. Near unity quantum yield of light-driven redox mediator reduction and efficient $H_2$ generation using colloidal nanorod heterostructures. *J. Am. Chem. Soc.* **2012**, *134*, 11701–11708.

[51] Gimbert-Suriñach, C.; Albero, J.; Stoll, T.; Fortage, J.; Collomb, M. N.; Deronzier, A.; Palomares, E.; Llobet, A. Efficient and limiting reactions in aqueous light-induced hydrogen evolution systems using molecular catalysts and quantum dots. *J. Am. Chem. Soc.* **2014**, *136*, 7655–7661.

[52] Ivanov, S. A.; Piryatinski, A.; Nanda, J.; Tretiak, S.; Zavadil, K. R.; Wallace, W. O.; Werder, D.; Klimov, V. I. Type-II core/shell CdS/ZnSe nanocrystals: Synthesis, electronic structures, and spectroscopic properties. *J. Am. Chem. Soc.* **2007**, *129*, 11708–11719.

[53] He, Y.; Zhang, M.; Shi, J. J.; Cen, Y. L.; Wu, M. Improvement of visible-light photocatalytic efficiency in a novel InSe/$Zr_2CO_2$ heterostructure for overall water splitting. *J. Phys. Chem. C* **2019**, *123*, 12781–12790.

[54] Bao, Y. P.; Wang, J.; Wang, Q.; Cui, X. F.; Long, R.; Li, Z. Q. Immobilization of catalytic sites on quantum dots by ligand bridging for photocatalytic $CO_2$ reduction. *Nanoscale* **2020**, *12*, 2507–2514.

[55] Bian, Z. F.; Tachikawa, T.; Zhang, P.; Fujitsuka, M.; Majima, T. A nanocomposite superstructure of metal oxides with effective charge transfer interfaces. *Nat. Commun.* **2014**, *5*, 3038.

[56] Huang, M. Y.; Li, X. B.; Gao, Y. J.; Li, J.; Wu, H. L.; Zhang, L. P.; Tung, C. H.; Wu, L. Z. Surface stoichiometry manipulation enhances solar hydrogen evolution of CdSe quantum dots. *J. Mater. Chem. A* **2018**, *6*, 6015–6021.

[57] Qiu, F.; Han, Z. J.; Peterson, J. J.; Odoi, M. Y.; Sowers, K. L.; Krauss, T. D. Photocatalytic hydrogen generation by CdSe/CdS nanoparticles. *Nano Lett.* **2016**, *16*, 5347–5352.

[58] Wang, P.; Wang, M. M.; Zhang, J.; Li, C. P.; Xu, X. L.; Jin, Y. D. Shell thickness engineering significantly boosts the photocatalytic $H_2$ evolution efficiency of CdS/CdSe core/shell quantum dots. *ACS Appl. Mater. Interfaces* **2017**, *9*, 35712–35720.